

BLUE STRAGGLER MASSES FROM PULSATION PROPERTIES. I. THE CASE OF NGC6541.

G. FIORENTINO¹, B. LANZONI¹, E. DALESSANDRO¹, F. R. FERRARO¹, G. BONO^{2,3}, M. MARCONI⁴

¹ Dipartimento di Fisica e Astronomia, Università degli Studi di Bologna, Viale Berti Pichat 6/2, 40127 Bologna, Italy

² Dipartimento di Fisica, Università di Roma Tor Vergata, Via della Ricerca Scientifica 1, 00133 Roma, Italy

³ INAF-Osservatorio Astronomico di Roma, Via Frascati 33, 00040 Monte Porzio Catone, Italy and

⁴ INAF-Osservatorio Astronomico di Capodimonte, Via Moiariello 16, 80131 Napoli, Italy

Draft version October 8, 2018

ABSTRACT

We used high-spatial resolution images acquired with the WFC3 on board HST to probe the population of variable blue straggler stars in the central region of the poorly studied Galactic globular cluster NGC 6541. The time sampling of the acquired multi wavelength (F390W, F555W and F814W) data allowed us to discover three WUma stars and nine SX Phoenicis. Periods, mean magnitudes and pulsation modes have been derived for the nine SX Phoenicis and their masses have been estimated by using pulsation equations obtained from linear non adiabatic models. We found masses in the range 1.0-1.1M_⊙, with an average value of 1.06 ± 0.09 M_⊙ ($\sigma = 0.04$), significantly in excess of the cluster Main Sequence Turn Off mass ($\sim 0.75M_{\odot}$). A mild trend between mass and luminosity seems also to be present. The computed pulsation masses turn out to be in very good agreement with the predictions of evolutionary tracks for single stars, indicating values in the range $\sim 1.0 - 1.2$ M_⊙ for most of the BSS population, in agreement with what discussed in a number of previous studies.

Subject headings: binaries: general; globular clusters: individual (NGC 6541); variables: SX Phoenicis

1. INTRODUCTION

Dense stellar environments like Galactic globular clusters (GCs) are populated by a large variety of *exotica*, including Blue Straggler Stars (BSSs), X-ray binaries, millisecond pulsars and cataclysmic variables (see Bailyn 1995; Pooley & Hut 2006; Paresce et al. 1992; Bellazzini et al. 1995; Ferraro et al. 2001; Ransom et al. 2005; Freire et al. 2008). Among them, BSSs certainly are the most numerous. They were discovered by Sandage (1953) in the outer regions of the Galactic GC M3 and, since then, they have been detected not only in GCs (see Piotto et al. 2004; Leigh et al. 2011), but also in open clusters (Mathieu & Geller 2009), and dwarf galaxies (Mateo et al. 1995; Mapelli et al. 2007; Monelli et al. 2012).

In the optical color magnitude diagram (CMD) BSSs are bluer and brighter than the main sequence (MS) turn-off (TO) stars, defining a sequence that typically spans more than 2-2.5 magnitudes above the cluster TO. Hence they mimic a younger stellar population with masses larger than normal cluster stars. Indeed, masses of the order of $M = (1.0 - 1.7)M_{\odot}$ have been estimated by direct measurements, although with large uncertainties (Shara et al. 1997; Gilliland et al. 1998; De Marco et al. 2005).

The origin of BSSs is still a matter of debate. They could be originated from collision-induced mergers, most likely in dense stellar environments (Hills & Day 1976; Leonard 1989), or by mass exchange in primordial binary systems (McCrea 1964; Zinn & Searle 1976; Knigge et al. 2009; Ferraro et al. 2006a,b). These two scenarios can possibly co-exist within the same cluster (Ferraro et al. 1995, 2009). Independently of their formation mechanism, BSSs are the brightest among the most massive stars in the host cluster and therefore are ideal tools to probe the dynamical evolution of stellar systems. Indeed, the observed shape of their radial distribution within the cluster has been recently used to define

the so-called "*dynamical clock*" (Ferraro et al. 2012), able to rank GCs on the basis of the dynamical stage reached. Since the engine of such a clock is dynamical friction and since the dynamical friction efficiency directly depends on the object mass, an accurate determination of BSS masses is of paramount importance for the calibration of such a clock.

Very interestingly, BSSs cross the faint extension of the classical Instability Strip (IS), where they are observed as SX Phoenicis stars (SXPs, see Pych et al. 2001; Jeon et al. 2003, 2004; McNamara 2011; Arellano Ferro et al. 2011). These objects show a photometric variability on very short periods ($P \lesssim 0.1$ d) and can be unstable for radial and non-radial pulsation. Hence, their pulsation properties can be used to estimate their masses. The Petersen's diagram (period ratio vs the longer period; Petersen 1978; Stellingwerf 1978; Gilliland et al. 1998), which is largely used for variable stars pulsating simultaneously in different modes, is very little sensitive to the mass in the period range typical of SXPs. However these variables follow the classical pulsation equation, relating the observed period to the intrinsic stellar parameters such as mass, luminosity and effective temperature $P(M, L, T_{\text{eff}})$, for any given pulsation mode and chemical composition. This relation can indeed be used to estimate the star mass, once the full set of variables is observed and/or assumed (Stellingwerf 1979; Da Costa et al. 1986; Marconi et al. 2004; Caputo et al. 2005; Fiorentino et al. 2006). For a precise determination of the pulsation equations, a complete theoretical scenario using a nonlinear and non adiabatic approach, also accounting for the convection, should be defined (Bono et al. 1997; Fiorentino et al. 2002; Marconi et al. 2005). This would be able to fully describe the pulsation properties of SXPs including their amplitudes and the red (cold) boundary of the IS. However, such a theoretical framework is still missing due to the huge amount of computation time necessary to integrate conservation equations for these high gravity pulsators. Nevertheless, theoretical models based on a radial, linear, non

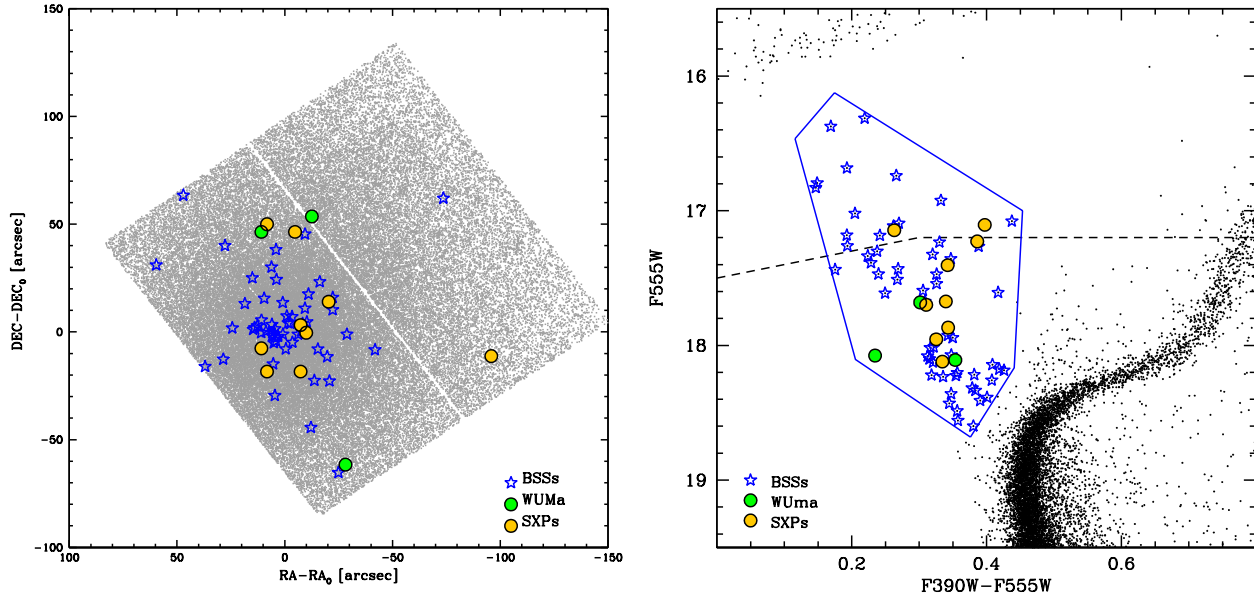


FIG. 1.— *left* – Map of the WFC3 data. The location of the selected BSSs is highlighted: blue starred symbols mark non-variable BSSs, green and orange circles indicate WUMa and SXP BSSs, respectively. Most of the selected BSSs are located in Chip#1, where the cluster center is also positioned. *right* – (F555W, F390W–F555W) CMD of NGC 6541 zoomed in the BSS region. The box used to select the BSS population is shown with blue contours. Non variable BSSs are marked as blue starred symbols, while variable BSSs are highlighted with green (WUMa) and orange (SXP) filled circles. The saturation limit of our dataset is also marked for reference (dashed line).

adiabatic approach to the stellar pulsation have been shown to reproduce quite confidently the SXP periods and the blue (hot) boundary of the IS (Stellingwerf 1979; Gilliland et al. 1998; Santolamazza et al. 2001), thus supporting the use of these approximated pulsation equations for the mass estimate. Attempts to estimate SXP masses have been performed using the pulsation equation based on Jorgensen & Hansen (1984) linear theoretical models, and masses of about $1.5 M_{\odot}$ up to twice the main sequence TO mass have been obtained for a sample of BSSs in NGC 5053 (Nemec et al. 1995).

In the present paper we use linear and non adiabatic theoretical pulsation models from Santolamazza et al. (2001) to estimate the mass of a sample of BSSs pulsating as SXPs in the Galactic globular cluster (GC) NGC 6541. This is an old (13.25 ± 1 Gyr Dotter et al. 2010) and metal-poor ($[Fe/H] = -1.76 \pm -0.02$, Lee & Carney 2002) GC with an extended blue Horizontal Branch (Dotter et al. 2010). It is located at 3 kpc from the Galactic Center and classified as a post-core collapse cluster (Harris 1996). Here new HST/WFC3 data are used to detect variable BSSs in the central region of NGC 6541. We found a sizeable sample of this exotic population and we discuss the mass determination for nine SXP pulsating BSSs.

The paper is organized as follows. The HST dataset and the data reduction procedure are described in Sec. 2. The BSS selection and their short-period variability study are described in Sec. 3. In Sec. 4 we present the method adopted to discriminate the pulsation mode of the nine selected SXPs, whereas in Sec. 6 we derive their mass. A discussion Section closes the paper.

2. OBSERVATIONS AND DATA REDUCTION

The data-set presented in this paper has been acquired using the UVIS channel of the HST/WFC3 on 2012 February 24 (PI: F. R. Ferraro, GO: 12516). The cluster is centered in chip#1 (see Fig. 1, left panel). The data set consists of twelve

F390W, ten F555W (narrow V) and thirteen F814W (wide I) frames. Each frame has been integrated for an exposure time of 348 s, 150 s and 348 s, respectively. The observing strategy includes a small dithering of a few pixels to correct CCD blemishes, artifacts and false detections. The three different filters were alternated during each orbit to optimize the final total exposure time.

The data reduction has been performed using DAOPHOT/ALLSTAR/ALLFRAME (Stetson 1987, 1994) on flat-fielded and bias subtracted (`_flt`) images once the pixel area map corrections were accounted for. The Point Spread Functions (PSFs) were derived on chip#1 and #2 separately using the brightest, isolated and non saturated stars. Typically, more than 600 stars were selected. These PSFs were used to perform ALLSTAR photometry in each frame. The obtained individual star lists have been combined using DAOMATCH in a single master list to run ALLFRAME. In this master list only stars appearing in at least 20 out of 35 images were included. Finally, the ALLFRAME output star lists were combined using DAOMASTER for each filter. For each star, we have homogenized the different magnitudes (e.g., Ferraro et al. 1991, 1992) to obtain their mean magnitudes and the corresponding time-series. The final list includes 72,616 stars.

In order to calibrate instrumental F390W, F555W and F814W magnitudes in the VEGAMAG photometric system we have followed the procedure described in Dalessandro et al. (2013), which includes Charge Transfer Efficiency correction for the WFC3 camera. A portion of the resulting (F555W, F390W–F555W) CMD, zoomed in the BSS region, is shown in Figure 1 (right panel). By following the same paper and according to the estimate of the UVIS channel performance, we have also computed the saturation threshold of our photometry. Following the instructions of the WFC3 Data Handbook, we used $72000 e^-$ as the value of the central pixel saturation and we adopted an aperture of 1×1 pixel for

the encircled energy in the three filters: $EE(F814W)=0.149$, $EE(F555W)=0.184$ and $EE(F390W)=0.180$. Then the flux close to saturation has been determined and transformed into magnitudes by applying the same equations used to calibrate our photometry in the HST VEGAMAG photometric system. The resulting saturation threshold is marked in Fig. 1 (right panel, dashed line).

Finally, to obtain a precise absolute astrometric solution we first accounted for geometric distortion following the prescriptions discussed in the WFC3 Data Handbook. Then, the instrumental positions of our stars have been cross correlated with a wide field catalog (P. B. Stetson, private communication) previously reported to the absolute astrometric system using the stars in common with the Guide Source Catalogue 2.3 (GSC2.3), by means of CataXcorr (see Dalessandro et al. 2011). Both the WFC3 and the wide field catalogs will be used in a forthcoming paper to properly determine the center and density profile of NGC 6541 and to constrain the mass and luminosity functions of this cluster.

3. BLUE STRAGGLER STAR SELECTION AND VARIABILITY SEARCH

The BSS population has been selected on the basis of the star location in the CMD (as objects bluer and brighter than the MS-TO), with conservative colour and magnitude limits aimed at reducing at most the contamination from stellar blends near the MS-TO and the sub-giant branch. In addition, a simultaneous check of the (F555W, F390W-F555W) and the (F555W, F555W-F814W) planes has been performed, and only stars located in the “appropriate” region in both CMDs have been selected as fiducial BSSs, following the general approach routinely adopted in previous papers (Ferraro et al. 2006a; Dalessandro et al. 2008). The resulting shape of the BSS selection box in the (F555W, F390W-F555W) plane is shown with blue contours in the right panel of Fig. 1. The final sample consists of 70 BSSs spanning ~ 2 mag in the F555W pass band and approaching the Horizontal Branch luminosity. The spatial distribution of these stars within NGC 6541 is shown in Fig.1 (left panel), revealing that they are well segregated in the cluster center (as quoted by Harris 1996, 2010 version).

As apparent from Fig. 1 (right panel), sixteen stars fall above the saturation threshold. However, all variable BSSs (green and orange circles; see below), which are the main targets of this study, are either below or very close to the saturation limit. Hence they are marginally affected by the photometric saturation. It is worth mentioning that, while possible variability signals may be hidden by saturation effects at brighter magnitudes, the most luminous BSSs are so blue that they unlikely cross the pulsation IS.

Our data sampling was collected within 13 HST orbits and consists of 35 images over a time interval of about 7 hours. However, thanks to the high photometric accuracy possible with HST (with errors $\sigma_{F390W} - \sigma_{F555W} - \sigma_{F814W} \lesssim 0.015$ mag at the BSS magnitude levels), it has been possible to perform a variability study and search for variable BSSs with short periods and relatively large amplitudes (e.g., $A_{F555W} \gtrsim 0.05$ mag), as already done for the case of NGC 362 (Dalessandro et al. 2013).

To this end, we have performed a Fourier time series analysis for all the selected BSSs in the three filters simultaneously by using GRATIS (GRaphical Analyzer of TIme Series, developed by P. Montegriffo at the INAF-Bologna Observatory; see Fiorentino et al. 2010a,b, and reference therein for

details). In particular, we have used low order Fourier coefficients to match the light curves in each pass band as a function of the phased Heliocentric Julian date. Only those stars showing variability with the same period within 1% in all the three filters were considered as *bona fide* variables. In particular, out of the 70 selected BSSs, nine stars with period smaller than 0.1 days have been identified as SXPs and three stars with period longer than 0.1 days were classified as WUMa stars. It is worth noticing that the detected sample of variable stars is far to be complete.

The phased light curves of the three WUMa stars are shown in Fig. 2 for the three filters. We remember here that WUMa stars are eclipsing binary systems. WUMa1 shows a not very sinusoidal behavior, with a flattening of the light curve at bright magnitudes due to the contribution of both the companions. The remaining two WUMa stars show, instead, a sinusoidal light curve typical of two very close components in a binary system. Our sample of SXPs shows sinusoidal light curves (see Figures 3-5), as expected in the case of an almost adiabatic behavior with large amplitudes. Despite the modest sampling of our data, we stress here that our classification stars as SXPs is fully supported by their pulsation properties, e.g. they follows a very tight and well defined PL relation (see Section 4).

Their amplitudes range from 0.06 to 0.39 mag in the F555W filter, and their periods varies from 0.032 to 0.065 days. We stress here that, due to both the photometric errors and the limited temporal sampling of our data, only high amplitude variations can be detected, and our SXP sample is therefore far to be complete. In addition, it is not possible to firmly assess the existence of more than one frequency, and in turn mixed mode pulsators can not be solidly recognized.

We derived the mean magnitudes of the detected variable stars using the truncated Fourier series that best match the data. The mean instrumental magnitudes were then calibrated using the same method adopted for non variable stars and described in the previous Section. The intensity-averaged mean magnitudes, periods, amplitudes and epochs (time at the maximum of the light curve) are listed in Table 1, together with the star coordinates. The position in the CMD of the detected SXP and WUMa stars, plotted according to the values given in Table 1 are shown in Fig. 1 (right panel).

4. PULSATION MODE IDENTIFICATION

In order to estimate the star mass from the pulsation equation, the first step is to determine the pulsation mode of the investigated variables. For well known pulsating stars crossing the IS, such as RR Lyrae, the first overtone (FO) mode pulsators show a more sinusoidal light curve with respect to the fundamental (F) mode pulsators. Moreover, the FO amplitudes are typically smaller than the F ones. Hence, the pulsation mode can be easily estimated from the morphology of the light curve. In those cases where these general rules are not easily applied, as for SXPs stars and Anomalous Cepheids, more detailed pulsation properties can also be adopted; e.g., the location in the period luminosity (PL) plane when variable stars are located at the same distance (Marconi et al. 2004; Fiorentino et al. 2006). We note that in the recent years, the SXP PL relation has been accurately investigated in several Galactic GCs (e.g. Pych et al. 2001; Jeon et al. 2003, 2004;

TABLE 1
PARAMETERS OF THE VARIABLE BSSs DETECTED IN NGC 6541.

ID	$\alpha_{J2000.0}$ deg	$\delta_{J2000.0}$ deg	Period days	Epoch (-2455900)	A_{F390W} mag	A_{F555W} mag	A_{F814W} mag	$\langle F390W \rangle$ mag	$\langle F555W \rangle$ mag	$\langle F814W \rangle$ mag	$\langle M/M_{\odot} \rangle$
WUMa1	272.014	-43.702	0.26 ± 0.04	80.850	0.45	0.45	0.34	18.46	18.11	17.62	"
WUMa2	271.999	-43.732	0.20 ± 0.02	81.450	0.14	0.12	0.09	17.98	17.68	17.26	"
WUMa3	272.005	-43.700	$\sim 0.44 \pm 0.10^d$	80.850	0.29	0.23	0.16	18.31	18.08	17.72	"
SXP1 ^F	272.002	-43.711	0.050 ± 0.001	80.970	0.29	0.26	0.16	18.01	17.67	17.21	1.03 ± 0.15
SXP2 ^{FO}	272.013	-43.701	0.0461 ± 0.003	80.959	$\gtrsim 0.12$	0.13	0.06	17.75	17.40	16.90	$1.27 \pm 0.18^F - 1.07 \pm 0.16^{FO}$
SXP3 ^F	272.007	-43.714	0.0649 ± 0.004	80.924	$\gtrsim 0.39$	0.44	0.25	17.61	17.20	16.76	1.13 ± 0.17
SXP4 ^F	272.006	-43.715	0.041 ± 0.003	80.956	$\gtrsim 0.06$	0.07	0.03	18.28	17.95	17.49	1.00 ± 0.15
SXP5 ^{F/FO}	272.007	-43.720	0.065 ± 0.002	80.980	$\gtrsim 0.27$	0.26	0.12	17.50	17.11	16.55	$1.23 \pm 0.18^F - 1.06 \pm 0.16^{FO}$
SXP6 ^F	272.014	-43.717	0.0425 ± 0.001	81.008	0.23	0.20	0.12	18.01	17.70	17.27	1.11 ± 0.16
SXP7 ^F	272.013	-43.720	0.032 ± 0.001	80.970	$\gtrsim 0.10$	0.13	0.04	18.46	18.12	17.65	1.05 ± 0.15
SXP8 ^F	272.008	-43.702	0.046 ± 0.002	80.985	0.10	0.08	0.05	18.21	17.87	17.36	0.98 ± 0.15
SXP9 ^{FO}	271.973	-43.718	0.059 ± 0.003	81.015	0.42	0.29	0.15	17.41	17.14	16.66	$1.27 \pm 0.19^F - 1.09 \pm 0.16^{FO}$

NOTE. — Name, coordinates, period, epoch, amplitude, mean magnitude for the WUMa and SXP stars identified in the BSS sample of NGC 6541. For the nine SXPs, also the likely pulsation mode (^{F/FO}) and the estimated pulsation mass are indicated (the latter corresponds to the average among the values obtained in the three filters; see Sect. 5). For those stars with uncertain mode classification, we have listed two possible values for the mass as computed using F or FO PL relations.^d This is the best period that match our data in the range 0.01–0.9 days. However, we note that our time sampling covers only 0.3 days, thus this value may be very uncertain.

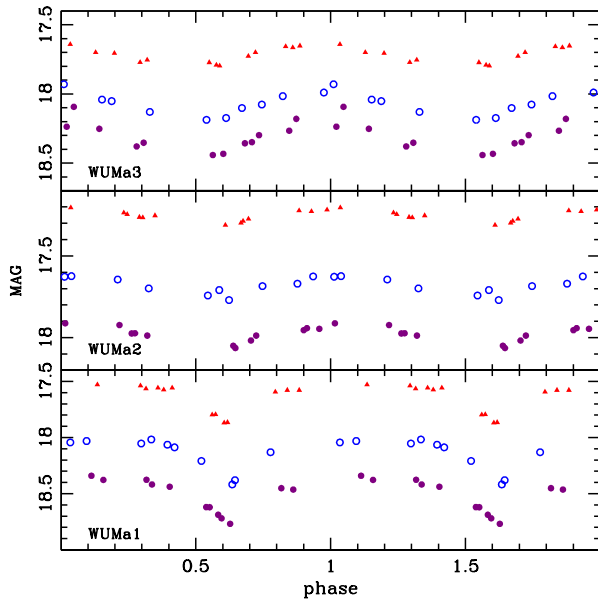


FIG. 2.— Phased light curves for the WUMa stars detected within our BSS sample. Different filters are color coded in each panel: purple light curve is for the F390W pass band, blue for the F555W and red for the F814W.

TABLE 2
PL-RELATIONS FOR FUNDAMENTAL
MODE PULSATORS.

FILTER	α	β	σ
M_{F390W}	-0.46	-2.70 ± 0.51	0.10
M_{F555W}	-0.95	-2.93 ± 0.53	0.11
M_{F814W}	-1.11	-2.87 ± 0.42	0.09

NOTE. — Numerical coefficients of the derived PL-relations expressed as $MAG = \alpha + \beta \times \log P$. The last column quotes the rms scatter of each relation.

McNamara 2011; Arellano Ferro et al. 2011, and reference therein) and in dwarf galaxies (e.g. LMC, Fornax, Carina, see Vivas & Mateo 2013) to determine the distance of the host stellar system. Here, instead, we use it only to determine the pulsation mode of our SXP sample, which is needed to esti-

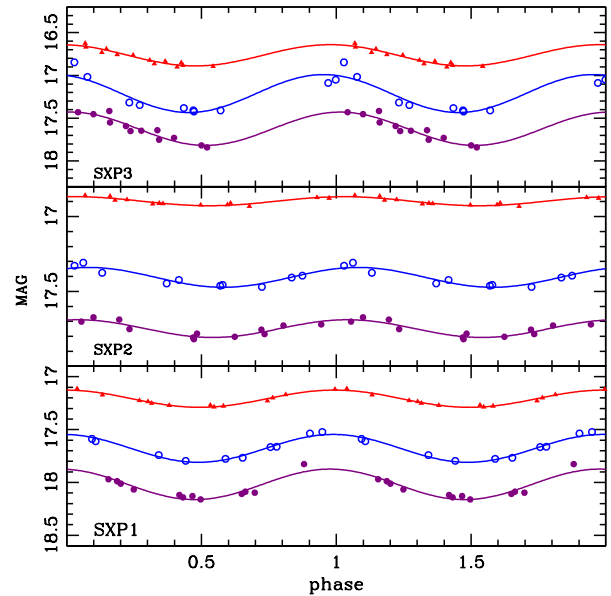


FIG. 3.— Phased light curves for three SXPs detected in our BSS sample. The color code is as in Fig. 2.

mate the SXP pulsation mass (see Section 5).

Empirical and theoretical results suggest significantly different periods for the F and the FO mode pulsations in SXPs, with a ratio $P_{FO}/P_F \sim 0.783$ (Santolamazza et al. 2001; Jeon et al. 2003; Arellano Ferro et al. 2011; Pych et al. 2001). Thus the two pulsation modes can be confidently distinguished in the Period-Absolute Magnitude plane. Indeed, abundant populations of SXPs in metal-poor GCs (21 SXPs with $[Fe/H] = -2.10$ in M53, and 24 SXPs at $[Fe/H] = -1.94$ in M55; Arellano Ferro et al. 2011; Pych et al. 2001, respectively) define two separate sequences well fitted, respectively, by the PL-relation derived for F mode pulsators (solid lines in Figure 6) and by the same relation shifted under the assumption $P_{FO}/P_F = 0.783$ (dotted lines).¹ We therefore used these relations to infer the pulsation mode of our SXPs, by assum-

¹ These relations have been obtained in the Johnson Kron-Cousins photometric system, we do not expect any large difference when using F555W and F814W magnitudes as in the case of classical Cepheids (Fiorentino et al. 2013).

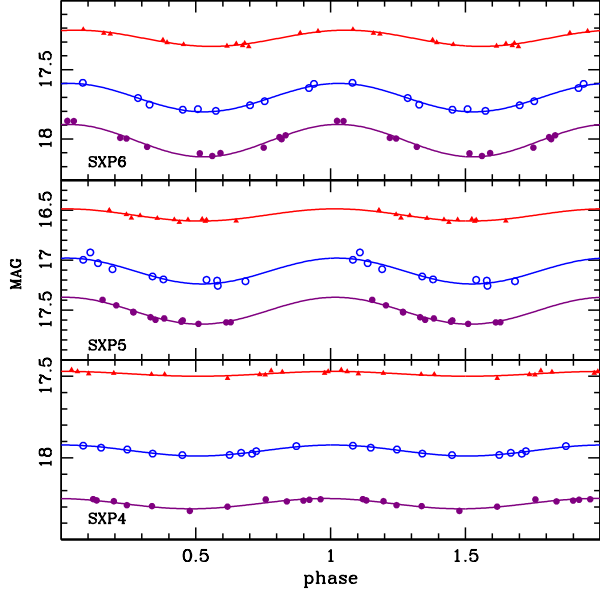


FIG. 4.— Same as in Fig. 3 for three other SXP BSSs.

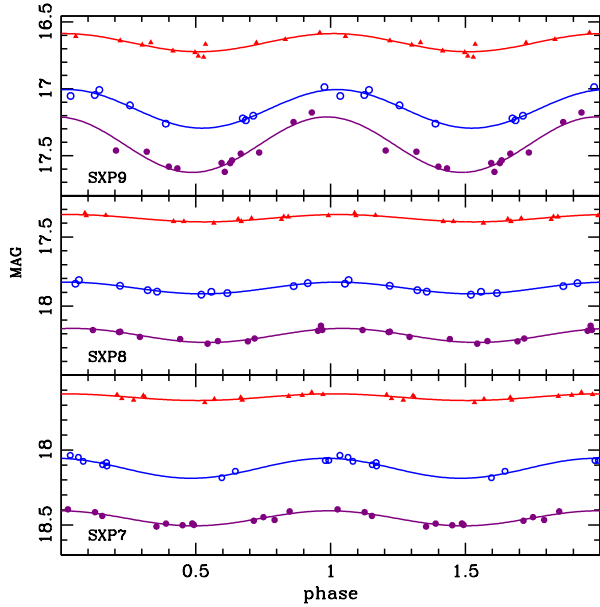


FIG. 5.— Same as in Fig. 3 for three other SXP BSSs.

ing a reddening $E(B-V) = 0.14$ mag (Cardelli et al. 1989) and a distance modulus $\mu_0 = 14.29$ mag (Lee & Carney 2002) for NGC6541.

As shown in Fig. 6, most of our variables follow the F mode PL relation in both the F555W (V) and the F814W (I) bands, with the possible exception of three stars, namely SXP2, SXP5 and SXP9. SXP2 and SXP9 seem to well follow the PL relations for FO mode pulsators in all the three filters. The case of SXP5 is more ambiguous being this star located close to the F mode PL relation in F390W and F555W pass-bands whereas it follows better the FO mode PL relation in the F814W filter. Here it is worth noticing that, since SXP5 has a quite large amplitude and its light curve is not fully covered by our data, its mean magnitude estimates may be not

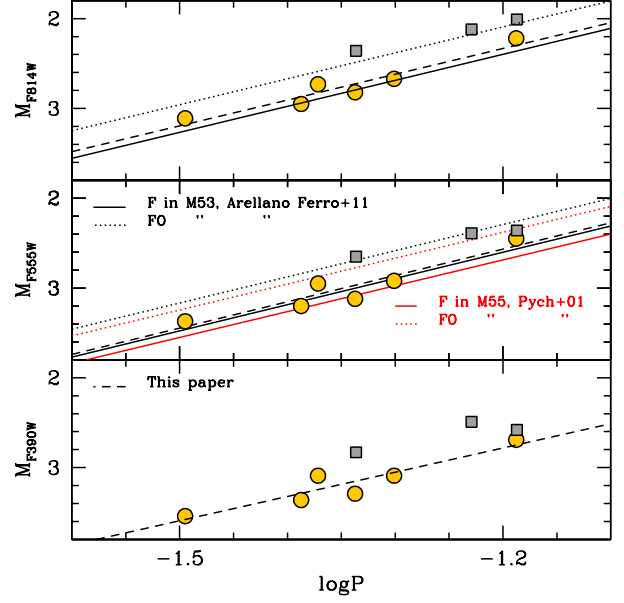


FIG. 6.— Location of the detected SXP BSSs (orange circles) in the Period-Absolute Magnitude plane, for the three available pass bands under the assumption of a reddening $E(B-V) = 0.14$ mag and a distance modulus $\mu_0 = 14.29$ mag (see Lee & Carney 2002). Orange circles and grey squares represent F and FO pulsators respectively. The solid lines represent the PL relations derived for the Fundamental (F) mode pulsators observed in M53 (black; Arellano Ferro et al. 2011) and in M55 (red; Pych et al. 2001). The dotted lines correspond to these relations shifted assuming $P_{FO}/P_F = 0.783$ and they mark the loci of the First Overtone (FO) pulsators. The dashed lines represent the best-fits to our data, derived by using only the likely F pulsators (see Section 4 for details).

TABLE 3
PULSATION EQUATIONS USED TO ESTIMATE THE STAR MASS.

FILTER	α	β	γ	δ	σ
F mode					
M_{F390W}	0.13	-0.18 ± 0.04	-0.38 ± 0.13	0.02 ± 0.01	0.04
M_{F555W}	0.05	-0.20 ± 0.04	-0.46 ± 0.13	0.01 ± 0.01	0.04
M_{F814W}	-0.27	-0.33 ± 0.05	-0.89 ± 0.15	0.01 ± 0.01	0.03
FO mode					
M_{F390W}	0.13	-0.14 ± 0.03	-0.26 ± 0.08	0.01 ± 0.01	0.04
M_{F555W}	0.04	-0.17 ± 0.03	-0.34 ± 0.09	0.01 ± 0.01	0.04
M_{F814W}	-0.31	-0.29 ± 0.03	-0.77 ± 0.11	0.01 ± 0.01	0.03

NOTE. — Numerical coefficients of the pulsation equations derived from linear non adiabatic models and expressed as $\log M/M_\odot = \alpha + \beta \times \text{MAG} + \gamma \log P + \delta \log Z/Z_\odot$.

very accurate. For this reason, in the following discussion we will consider that SXP5 can be classified either as F or FO pulsator.

Finally, we found a quite good agreement (in terms of both the slopes and the zero points) between the linear fit to our likely F pulsators (dashed lines in Fig. 6 and Table 2) and the relations quoted by Pych et al. (2001) and Arellano Ferro et al. (2011). Hence, we can reasonably use our data to determine, for the first time, the PL relation of SXPs in the F390W-band (see bottom panel of Fig. 6 and Table 2).

5. PULSATION MASSES

Once the pulsation modes of our SXP sample have been determined (Sect. 4), we estimate the BSS mass through pul-

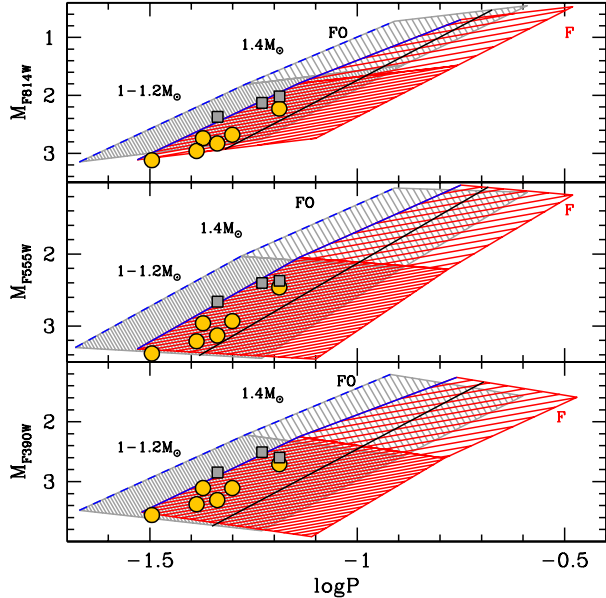


FIG. 7.— Grids of linear non adiabatic models (from Santolamazza et al. 2001) in the Period-Absolute Magnitude plane for the available set of filters. Red and grey colors correspond to models computed for F and FO mode pulsators, respectively. Narrow and large shadings correspond to different masses: $1.0\text{--}1.2 M_{\odot}$ and $1.4 M_{\odot}$ respectively. The blue lines represent the theoretical Fundamental (solid) and First-Overtone (dashed) Blue Edges of the IS. The black solid lines mark the empirical red edge of the IS adopted “ad hoc” for deriving the theoretical PL relations, see the text for details. SXPs are shown for comparison with the same symbols as in Fig. 6.

sation equations $P(M, L, T_{\text{eff}})$ derived from the linear and non adiabatic pulsation models of Santolamazza et al. (2001) for the first two modes. In that paper, the authors present a grid of models assuming three values for the star mass (1.0 , 1.2 and $1.4 M_{\odot}$) and two different metallicities ($[\text{Fe}/\text{H}] = -2.2$ and -1.3 dex) that bracket the iron abundance of NGC 6541 ($[\text{Fe}/\text{H}] = -1.76$; Lee & Carney 2002). For each mass, several luminosity levels are adopted. The models also span a large range in effective temperatures to reproduce the extension of the IS. However, the major limit of the adopted models is that they do not account for the efficiency of the convection flux during the pulsation. This becomes especially important at cold effective temperatures ($T_{\text{eff}} \sim 6000\text{K}$ for the SXPs mass range), where convection can balance the temperature gradient in the stellar envelope, with the final effect of quenching the stellar pulsation. This means that the linear non adiabatic approach is unable to predict the location of the red boundary of the IS and the explored temperatures cover a large range arbitrarily fixed by the authors. To overcome this limitation, we decide to adopt the *observed* red boundary of the IS, which seems to be a quite reasonable assumption.

In order to compare the models with our data we have transformed the theoretical luminosities and effective temperatures into the VEGAMAG HST photometric system, as described in Fiorentino et al. (2013). The region covered by the grid of F and FO models in the PL plane is shown in Fig. 7 for the three filters. The red and grey colors indicate the F and FO modes, respectively, and the two different shading indicate models with masses $1.0\text{--}1.2$ and $1.4 M_{\odot}$. These regions become narrower and steeper moving towards longer wavelengths (from F390W to F814W). Our observations are shown for comparison and clearly define a very narrow region in period at fixed luminosity, whereas the models span a larger period range. As

mentioned above, this is a fictitious consequence of using a linear non adiabatic approach. To better constrain the models, the red boundary of the IS is empirically fixed at *de-reddened* colors (F555W–F814W) ~ 0.4 mag (see the black lines shown in Fig. 7) which corresponds to the location in the CMD of the reddest SXPs *observed* in our sample as well as in that of NGC5024 Arellano Ferro et al. (2011) with similar metallicity.

To construct the pulsation equations we therefore used only the models bluer than this limit and, owing to the limited range in colour, we also neglected the temperature dependence. Within these assumptions, for each selected filter and pulsation mode, the grid of available models allowed us to derive pulsation equations of the form $\log M/M_{\odot} = \alpha + \beta \times \text{MAG} + \gamma \log P + \delta \log Z/Z_{\odot}$, with the values of the coefficients listed in Table 3.

While the visual inspection of Fig. 7 already suggests that the observed variable BSSs have masses consistent with $1.0\text{--}1.2 M_{\odot}$, the derived relations have been used to estimate the mean mass and the dispersion for each star using the observational data in the three pass bands. The results are listed in Table 1 and summarized in Fig. 8, where masses are plotted as a function of magnitudes in the three pass bands and errorbars are estimated from the photometric uncertainty on the mean magnitudes and the dispersion σ of the adopted relations (last column of the Table 1). In each panel we also give the mean mass value with its error computed on the whole sample, assuming SXP2, SXP5 and SXP9 as FO pulsators. The standard deviation is also indicated to highlight the very good stability of the data around the mean.

Given the large uncertainty in the mode classification, we have estimated the masses for SXP2, SXP5 and SXP9 also using the F mode classification and the results are listed in Table 1. Moreover, the arrows in Fig. 8 start at the mass values obtained assuming SXP2, SXP5 and SXP9 as FO pulsators and end at those computed adopting the F mode classification. When we assume all the stars as F pulsators, the mean mass values listed in each panel of Fig. 8 slightly increase together with their standard deviation, i.e. $\langle M/M_{\odot}(\text{F390W}) \rangle = 1.13 \pm 0.10$ ($\sigma = 0.10$), $\langle M/M_{\odot}(\text{F555W}) \rangle = 1.12 \pm 0.10$ ($\sigma = 0.10$) and $\langle M/M_{\odot}(\text{F814W}) \rangle = 1.10 \pm 0.08$ ($\sigma = 0.15$).

6. DISCUSSION AND CONCLUSIONS

We have used linear non adiabatic pulsation models (Santolamazza et al. 2001) to estimate the mass of the detected SXP BSSs as a function of their observed mean magnitude, period and metallicity. As expected, we found that all the investigated SXP BSSs have (pulsation) masses larger than the stellar mass at the MS-TO ($\sim 0.75 M_{\odot}$), as determined from α -enhanced evolutionary tracks at the cluster metallicity, computed from the BASTI database (Pietrinferni et al. 2004). Within the errors, the obtained results are compatible with an average mass $\langle M/M_{\odot} \rangle \sim 1.06 \pm 0.09$ ($\sigma = 0.04$). However, Fig. 8 shows a mild trend between mass and luminosity, especially if considering the two pass bands (F555W and F390W) with the highest photometric accuracy (F814W, instead, is significantly more affected by saturation problems). This is best appreciable in Fig. 9, where we have grouped the nine SXPs in three magnitude bins and computed their average pulsation mass (see the horizontal black segments and the corresponding labels in the figure). This trend is even stronger when we classify the whole sample of SXPs as formed by F pulsators. In fact, the mean

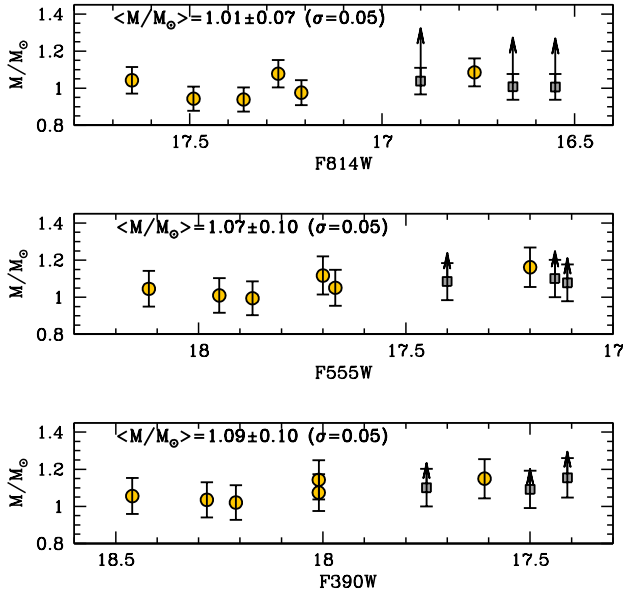


FIG. 8.— Pulsation masses as a function of magnitude for the nine SPX BSSs, estimated from the pulsation equations listed in Table 3 (see Section 5 for details). The mean values of the mass obtained in the three pass bands are labelled in each panel together with their error and their standard deviation. Symbols are the same used in Fig. 6. Arrows point at the mass values derived when F PL relations are used for stars with uncertain mode classification.

mass in each magnitude bin would be 1.01, 1.14 and 1.21 M_{\odot} going from faint to brighter magnitudes.

In the same Fig. 9, the position in the CMD of our SXP BSSs is compared to that of α -enhanced evolutionary tracks (Pietrinferni et al. 2004) computed for 1.0, 1.1 and 1.2 M_{\odot} stars at the cluster metallicity and assuming the same reddening and a distance modulus quoted above. These tracks bracket the location of our SXPs, thus suggesting a very narrow range for the evolutionary mass, with a mean value $\langle M_{\text{evo}} \rangle = 1.1 \pm 0.1 M_{\odot}$ which is in excellent agreement with the pulsation estimate. A similar good agreement has been discussed by Gilliland et al. (1998) using the pulsation properties of three mixed-mode SXPs in 47Tuc. These authors compared their observations in the Petersen diagram with the same pulsation linear models used here (Santolamazza et al. 2001). However, they also found a significant discrepancy for one of the four analysed mixed-mode SXPs that turns out to have a pulsation mass 20% smaller than the evolutionary one.

In the last years, a variety of approaches have been used to estimate the mass of BSS stars in globular and open clusters. The first direct measurement of one of the most luminous BSS in the core of 47 Tuc has been presented by Shara et al. (1997) through a spectroscopic analysis of FOS@HST data. The derived mass (1.7 M_{\odot}) is twice the cluster’s MS-TO mass and agrees well with the estimate obtained using theoretical stellar evolutionary tracks for single star. In a subsequent study, using low- and intermediate-resolution spectroscopy in a number of GCs (NGC6752, NGC5272 and NGC6397), De Marco et al. (2005) found that the mean BSS masses for individual clusters (1.27, 1.05, 0.99, and 0.99 M_{\odot} , respectively) were significantly lower than the values expected by evolutionary theory. However, this discrepancy can be accounted for by the large errors in their mass evaluations. Only recently, very accurate mass estimates have been possible through spectroscopic and photometric analysis of eclips-

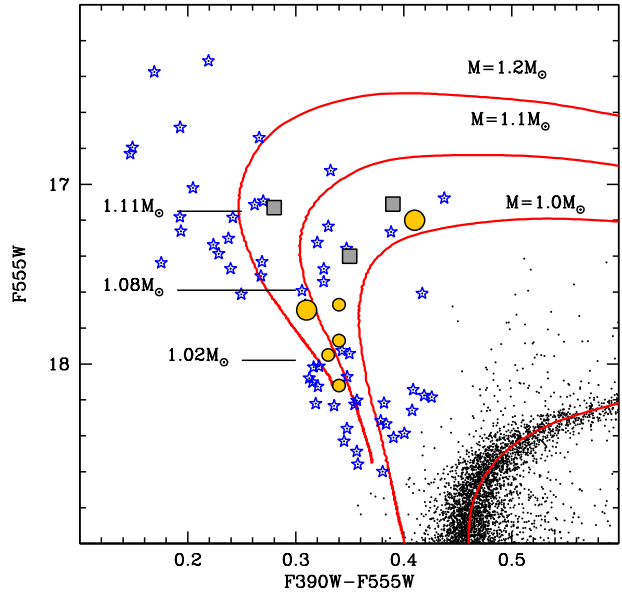


FIG. 9.— (F555W, F390W-F555W) CMD zoomed in the BSS region with highlighted the SXP BSSs (symbols as in Fig. 6). The size of the symbols reflects the value of the estimated pulsation mass. The horizontal black segments indicate the mean masses (see labels) obtained by grouping the nine SXPs in three bins of increasing magnitude, and they are positioned in correspondence of the mean magnitude of each bin. Evolutionary tracks for single stars with masses equal to 1.0, 1.1 and 1.2 M_{\odot} (from Pietrinferni et al. 2004) are also shown for comparison.

ing binaries in three GCs, i.e. 47 Tucanae (Thompson et al. 2010), ω Centauri, NGC6752 (Kaluzny et al. 2007a,b, 2009) supporting the agreement between these masses and those predicted from single star evolutionary tracks. The only exception is BSS V209 in ω Centauri that shows a larger mass ($\sim 0.95 M_{\odot}$) than MS-TO stars ($\sim 0.75 M_{\odot}$), but smaller than what expected from the comparison between evolutionary tracks and its bright and blue location in the CMD (~ 1.2 -1.3 M_{\odot} , see Kaluzny et al. 2007a; Ferraro et al. 2006a, for more details). Finally, more recent observations devoted to the study of a double-lined binary BSS in the not so young (~ 7 Gyr old) open cluster NGC188 (Geller & Mathieu 2012) indicate that single star evolutionary models overestimate (by 15-30%) the dynamical mass.

While the reasons for some of the observed discrepancies need to be clarified, the results here discussed indicate that single star evolutionary tracks can be safely used to estimated the BSS mass and suggest values below $\sim 1.2 M_{\odot}$ for most of the population, in agreement with what argued in a number of previous studies (e.g. Ferraro et al. 2006b; Lanzoni et al. 2007). We also note that, for BSSs close to the zero age MS, masses are more precisely constrained by pulsation models, since stellar evolutionary tracks become degenerate in that region of the CMD.

We conclude the paper by critically discussing the limitations of the adopted approach. The models of Santolamazza et al. (2001) are suitable for radial pulsators. Indeed, the relatively large amplitude of the variations observed ($A_{F555W} \gtrsim 0.05$ mag) and the period ratio measured in double mode pulsators support the hypothesis that most SXPs are radially pulsating stars (as discussed in Stellingwerf 1979). Moreover, despite a linear and non adiabatic approach to the stellar pulsation, the models have been shown to well

reproduce the SXP periods and the blue boundary of the IS (Stellingwerf 1979; Gilliland et al. 1998; Santolamazza et al. 2001). In order to have a full description of the radial stellar pulsation, non linear equations have to be solved, including a treatment for the coupling between pulsation and convection. Once available, these models will allow us to address crucial open questions like the dependency of SXP pulsation on masses, luminosities and chemical content, providing new tools to be used to better constrain the pulsation masses of SXPs. We will have at disposal more precise Period–Luminosity, Period–Luminosity–Color relations and, more interestingly, we will be able to accurately predict the amplitudes and the morphology of the SXP light curves. We

have started the computation of non linear models for SXP stars extending our theoretical scenario to low masses and for different metallicities. As described in Bono et al. (2002), this requires very long computation time and results will be presented in forthcoming papers, where we plan to apply this new theoretical approach to all BSSs for which reliable mean magnitudes and periods can be measured.

ACKNOWLEDGMENTS

This research is part of the project Cosmic-Lab (<http://www.cosmic-lab.eu>) funded by the European Research Council under contract ERC-2010-AdG-267675.

REFERENCES

- Arellano Ferro, A., Figuera Jaimes, R., Giridhar, S., Bramich, D. M., Hernández Santisteban, J. V., & Kuppuswamy, K. 2011, *MNRAS*, 416, 2265
- Bailyn, C. D. 1995, *ARA&A*, 33, 133
- Bellazzini, M., Pasquali, A., Federici, L., Ferraro, F. R., & Pecci, F. F. 1995, *ApJ*, 439, 687
- Bono, G., Caputo, F., Cassisi, S., Castellani, V., & Marconi, M. 1997, *ApJ*, 479, 279
- Bono, G., Caputo, F., Marconi, M., & Santolamazza, P. 2002, in *Astronomical Society of the Pacific Conference Series*, Vol. 256, *Observational Aspects of Pulsating B- and A Stars*, ed. C. Sterken & D. W. Kurtz, 249
- Caputo, F., Bono, G., Fiorentino, G., Marconi, M., & Musella, I. 2005, *ApJ*, 629, 1021
- Cardelli, J., Clayton, G., & Mathis, J. 1989, *ApJ*, 345, 245
- Da Costa, G. S., Norris, J., & Villumsen, J. V. 1986, *ApJ*, 308, 743
- Dallessandro, E., Lanzoni, B., Beccari, G., Sollima, A., Ferraro, F. R., & Pasquato, M. 2011, *ApJ*, 743, 11
- Dallessandro, E., Lanzoni, B., Ferraro, F. R., Vespe, F., Bellazzini, M., & Rood, R. T. 2008, *ApJ*, 681, 311
- Dallessandro, E., et al. 2013, *ArXiv e-prints*
- De Marco, O., Shara, M. M., Zurek, D., Ouellette, J. A., Lanz, T., Saffer, R. A., & Sepinsky, J. F. 2005, *ApJ*, 632, 894
- Dotter, A., et al. 2010, *ApJ*, 708, 698
- Ferraro, F. R., Clementini, G., Fusi Pecci, F., & Buonanno, R. 1991, *MNRAS*, 252, 357
- Ferraro, F. R., D’Amico, N., Possenti, A., Mignani, R. P., & Paltrinieri, B. 2001, *ApJ*, 561, 337
- Ferraro, F. R., Fusi Pecci, F., & Bellazzini, M. 1995, *A&A*, 294, 80
- Ferraro, F. R., Fusi Pecci, F., & Buonanno, R. 1992, *MNRAS*, 256, 376
- Ferraro, F. R., Sollima, A., Rood, R. T., Origlia, L., Pancino, E., & Bellazzini, M. 2006a, *ApJ*, 638, 433
- Ferraro, F. R., et al. 2006b, *ApJ*, 647, L53
- 2009, *Nature*, 462, 1028
- 2012, *Nature*, 492, 393
- Fiorentino, G., Caputo, F., Marconi, M., & Musella, I. 2002, *ApJ*, 576, 402
- Fiorentino, G., Limongi, M., Caputo, F., & Marconi, M. 2006, *A&A*, 460, 155
- Fiorentino, G., Musella, I., & Marconi, M. 2013, *ArXiv e-prints*
- Fiorentino, G., et al. 2010a, *ApJ*, 711, 808
- 2010b, *ApJ*, 708, 817
- Freire, P. C. C., Wolszczan, A., van den Berg, M., & Hessels, J. W. T. 2008, *ApJ*, 679, 1433
- Geller, A. M., & Mathieu, R. D. 2012, *AJ*, 144, 54
- Gilliland, R. L., Bono, G., Edmonds, P. D., Caputo, F., Cassisi, S., Petro, L. D., Saha, A., & Shara, M. M. 1998, *ApJ*, 507, 818
- Harris, W. E. 1996, *AJ*, 112, 1487
- Hills, J. G., & Day, C. A. 1976, *Astrophys. Lett.*, 17, 87
- Jeon, Y.-B., Lee, M. G., Kim, S.-L., & Lee, H. 2003, *AJ*, 125, 3165
- 2004, *AJ*, 128, 287
- Jorgensen, H. E., & Hansen, L. 1984, *A&A*, 133, 165
- Kaluzny, J., Rozycka, M., Thompson, I. B., & Zloczewski, K. 2009, *AcA*, 59, 371
- Kaluzny, J., Rucinski, S. M., Thompson, I. B., Pych, W., & Krzeminski, W. 2007a, *AJ*, 133, 2457
- Kaluzny, J., Thompson, I. B., Rucinski, S. M., Pych, W., Stachowski, G., Krzeminski, W., & Burley, G. S. 2007b, *AJ*, 134, 541
- Knigge, C., Leigh, N., & Sills, A. 2009, *Nature*, 457, 288
- Lanzoni, B., et al. 2007, *ApJ*, 663, 1040
- Lee, J.-W., & Carney, B. W. 2002, *AJ*, 124, 1511
- Leigh, N., Sills, A., & Knigge, C. 2011, *MNRAS*, 415, 3771
- Leonard, P. J. T. 1989, *AJ*, 98, 217
- Mapelli, M., Ripamonti, E., Tolstoy, E., Sigurdsson, S., Irwin, M. J., & Battaglia, G. 2007, *MNRAS*, 380, 1127
- Marconi, M., Fiorentino, G., & Caputo, F. 2004, *A&A*, 417, 1101
- Marconi, M., Musella, I., & Fiorentino, G. 2005, *ApJ*, 632, 590
- Mateo, M., Fischer, P., & Krzeminski, W. 1995, *AJ*, 110, 2166
- Mathieu, R. D., & Geller, A. M. 2009, *Nature*, 462, 1032
- McCrea, W. H. 1964, *MNRAS*, 128, 147
- McNamara, D. H. 2011, *AJ*, 142, 110
- Monelli, M., et al. 2012, *ApJ*, 744, 157
- Nemec, J. M., Mateo, M., Burke, M., & Olszewski, E. W. 1995, *AJ*, 110, 1186
- Paresce, F., de Marchi, G., & Ferraro, F. R. 1992, *Nature*, 360, 46
- Petersen, J. O. 1978, *A&A*, 62, 205
- Pietrinferni, A., Cassisi, S., Salaris, M., & Castelli, F. 2004, *ApJ*, 612, 168
- Piotto, G., et al. 2004, *ApJ*, 604, L109
- Pooley, D., & Hut, P. 2006, *ApJ*, 646, L143
- Pych, W., Kaluzny, J., Krzeminski, W., Schwarzenberg-Czerny, A., & Thompson, I. B. 2001, *A&A*, 367, 148
- Ransom, S. M., Hessels, J. W. T., Stairs, I. H., Freire, P. C. C., Camilo, F., Kaspi, V. M., & Kaplan, D. L. 2005, *Science*, 307, 892
- Sandage, A. R. 1953, *AJ*, 58, 61
- Santolamazza, P., Marconi, M., Bono, G., Caputo, F., Cassisi, S., & Gilliland, R. L. 2001, *ApJ*, 554, 1124
- Shara, M. M., Saffer, R. A., & Livio, M. 1997, *ApJ*, 489, L59
- Stellingwerf, R. F. 1978, *ApJ*, 224, 953
- 1979, *ApJ*, 227, 935
- Stetson, P. B. 1987, *PASP*, 99, 191
- 1994, *PASP*, 106, 250
- Thompson, I. B., Kaluzny, J., Rucinski, S. M., Krzeminski, W., Pych, W., Dotter, A., & Burley, G. S. 2010, *AJ*, 139, 329
- Vivas, A. K., & Mateo, M. 2013, *ArXiv e-prints*
- Zinn, R., & Searle, L. 1976, *ApJ*, 209, 734